In-situ borehole temperature measurements confirm dynamics of the gas hydrate stability zone at the upper Danube deep sea fan, Black Sea

Michael Riedel[1*], Tim Freudenthal[2], Jörg Bialas[1], Cord Papenberg[1], Matthias Haeckel[1], Markus Bergenthal[2], Thomas Pape[2,3], and Gerhard Bohrmann[2,3]

[1] GEOMAR Helmholtz Centre for Ocean Research Kiel, Wischhofstrasse 1 – 3, 24148 Kiel, Germany

[2] MARUM - Center for Marine Environmental Sciences, University Bremen, Leobener Str. 8, 28359 Bremen, Germany

[3] Faculty of Geosciences, University of Bremen, Klagenfurter Str. 2 – 4, 28334 Bremen, Germany

Abstract

Coring, geophysical logging, and in-situ temperature measurements were performed with the MARUM-MeBo200 seafloor rig to characterize gas hydrate occurrences in sediments of the Danube deep sea fan, off Romania, Black Sea. The new drilling data showed no evidence for significant gas hydrate saturations within the sediments but the presence of free gas at the depth of the bottom-simulating reflector (BSR). In-situ temperature and core-derived geochemical data suggest that the current base of the gas hydrate stability zone (BGHSZ) is ~20 m shallower than the BSR. Investigation of the seismic data around the drill sites shows several locations where free gas previously trapped at a former BGHSZ migrated upwards forming a new reflection above the BSR. This shows that the gas hydrate system in the Danube deep sea fan is still responding to climate changes initiated at the end of the last glacial maximum.

Keywords

In-situ temperature measurements, gas hydrates, bottom-simulating reflector, Black Sea, seafloor drilling rig

1 Introduction

Since the initial discovery of gas hydrates in the Black Sea in 1974 (Yefremova and Zhizchenko, 1974) a number of projects were conducted studying the occurrence of gas hydrates along the continental margins of the Black Sea (Ginsburg, 1998; Vassilev, 2002; Bohrmann et al., 2003; Minshull et al., 2020). Work included various seismic studies (Popescu et al., 2010; Bialas et al., 2014; Küçük et al., 2015; Hillman et al., 2018a,b) to map bottom-simulating reflectors (BSRs), which are used as an indicator for the base of the structure I (sI) gas hydrate stability zone (BGHSZ) (Shipley et al., 1979; Spence et al., 2010). BSRs are generally not widely distributed in the Black Sea (Ginsburg, 1998; Popescu et al., 2007), but unique stacks of up to five BSRs across thick sediment deposits of various channel-systems of the Danube deep-sea fan region were linked to former climate conditions (Popescu et al., 2006). An alternative explanation of structure II gas hydrate from deeply-rooted gas occurrences was provided (Baristeas, 2006). However, more recent modelling (Zander et al., 2017) confirmed that temperature and water level variations during glacial and inter-glacial climate epochs can best explain the multiple BSRs.

Numerous active gas expulsion sites and gas hydrate bearing cold vents were found in various regions of the Black Sea (Klaucke et al., 2006; Naudts et al., 2006; Greinert et al., 2010; Pape et al., 2011; Römer et al., 2020; Riboulot et al., 2017). According to current temperature and salinity conditions in the Black Sea gas hydrate is stable in water depths greater than ~720 m (Naudts et al., 2006; Pape et al., 2010). Abundant gas seepage is thus primarily found at shallower water depths than this threshold (Naudts et al., 2006; Riboulot et al., 2017; Römer et al., 2020).

Drilling and coring was performed in the Black Sea basin as part of the Deep Sea Drilling Project (DSDP) at Site 379, setting the background sedimentological and geochemical constraints of the uppermost 200 to 300 meter of sediment below seafloor (Ross et al., 1978). Additional deep piston coring and geotechnical probing up to ~24 meter below seafloor (mbsf) were performed at the Danube deep sea fan during the GHASS project in 2015 (Ker at al., 2015). To further study gas hydrates in the region, drilling with the MARUM-MeBo200 seafloor drill rig (Freudenthal and

Wefer, 2013) was performed at three sites (Table 1) off the Romanian shelf in 2017 from the German research vessel (R/V) METEOR during expedition M142 (Figure 1) in the frame of the German SUGAR project (Bohrmann et al., 2018). Drilling was set to obtain sediment cores to depths near the BGHSZ and characterize the gas hydrate occurrences within channel-levee sediments believed to exhibit favourable conditions for higher-concentrated accumulations following the gas hydrate petroleum system model (Collett et al., 2009). During this drilling, the first gas hydrate related geophysical logging and in-situ temperature measurements in the Danube deep sea fan were performed with the MeBo200 (Bohrmann et al., 2018).

Here, we report on the results of these measurements and implications on the gas hydrate stability zone in the region. The in-situ temperature data are combined with pore fluid chemistry from recovered sediments together with the drilling-derived gas composition (Pape et al., 2020) to predict the BGHSZ and integrate those findings with the wealth of seismic data in the region (Figure 1). Results are then put into the context of the changes in the Black Sea oceanographic conditions since the last glacial maximum (LGM) around 20 ka ago, when bottom water temperature was near 4 °C and sea level was ~100 m lower than today (Soulet et al., 2010; Constantinescu et al., 2015).

Earlier work in the region had shown a depth-discrepancy between the modelled (steady state) BGHSZ and seismically imaged BSR (Riboulot et al., 2017; Ker et al., 2019; Riboulot et al., 2018), with the BSR being generally too deep for todays' condition (Ker et al., 2019). No definitive test of any possible scenario explaining these discrepancies (e.g. transient state of the thermal regime, anomalous pore pressures, lateral strong variation in heat flow) exists so far due to the lack of deep drilling information (salinity, gas chemistry, in-situ temperature to depth of the BSR), and significant uncertainties in the parameters required to define the depth of the BGHSZ from seismic data (i.e., P-wave velocity, Riedel et al., 2020). Here, we can demonstrate that the seismically imaged BSRs are not indicating the BGHSZ given present conditions in the Black Sea but reflect a previous geologic period of stable pressure and temperature conditions, conditions occurring maybe during or shortly after the LGM (Soulet et al., 2010; Constantinescu et al., 2015). A new, but patchy, seismic reflection has developed where permeability barriers can be overcome locally, thus indicating the current shallowest depth of free gas and therefore the local BGHSZ. These shallower BSR-like reflections have not been reported prior to our new study. Gas migration occurs in part along more permeable strata which appears amplified along the eastward shoulders of channel-levee deposits. Using the available P-cable 3D data (Bialas et al., 2014; Hillman et al., 2018a, b) around the new MeBo drilling sites and deriving similarity attributes we also show evidence for fault-controlled upward gas migration.

Table 1. Overview of MeBo drilling sites and gravity core location with water depth, depth of seismically inferred BSR, and maximum coring depth reached.

Site	Latitude N	Longitude E	Water depth (m)	Maximum drilling depth (mbsf)	BSR depth (mbsf)
GeoB22605-1 MeBo-17	43°56.90’	30°47.01’	765	144.1	144
GeoB22620-1 MeBo-19	43°56.90’	30°47.01’	780	134.7	144
GeoB22603-1 MeBo-16	43°55.95’	30°49.75’	860	147.3	202
GeoB2209-2 MeBo-18	43°52.83’	30°52.67’	1,400	17.9	n.d.
GeoB22610-1 GC4	43°55.92‘	30°49.76‘	780	7.56	144
GeoB22611-1 GC5	43°56.90‘	30°47.02‘	765	7.90	202

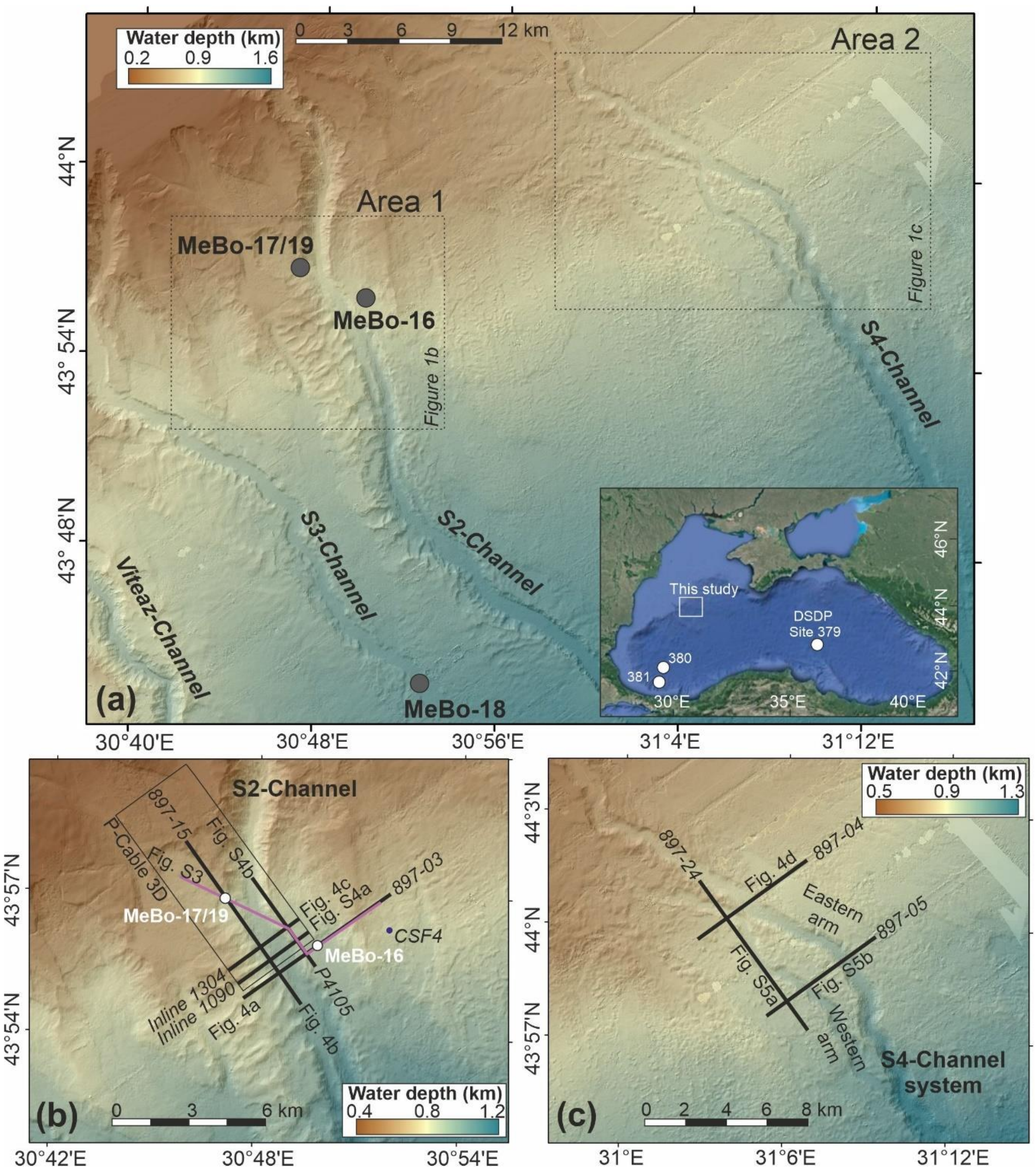

Figure 1 Seafloor bathymetric map of the study region. Two regions with patchy distributions of anomalous bottom simulating reflections (BSRs) are outlined with black boxes and shown in detail in (b) and (c). Inset shows study region (white box) in the western Black Sea and the Deep Sea Drilling Program (DSDP) Sites 379 - 381 (Ross et al., 1978). (b) Area 1 at the S2-channel with MeBo drill sites and station CSF4 (Calypso Flux coring system) from GHASS expedition (Riboulot et al., 2018). (c) Area 2 around S4-channel showing locations of 2D multichannel seismic lines utilized (Bialas et al., 2014).

2 Materials and Methods

2.1 Temperature measurements

In-situ temperatures were determined at twelve depth-intervals at Site GeoB22605-1 (MeBo-17) and at 14.35 mbsf at Site GeoB22609-2 (MeBo-18) (Figure 2; Table S1). The measurement principle is based on inserting a miniature temperature logger (MTL, Pfender and Villinger, 2002) into the sediment and determining the in-situ temperature by analysing the decay of temperature after an initial frictional heating pulse (Figures S1, S2). The MTL used during the MeBo-17 deployment was calibrated by comparing the readings of the sensor with a Conductivity-Temperature-Depth (CTD) probe also attached to the frame of the MeBo drill-rig. The calibration showed an offset of 0.017 (±0.001) °C between the CTD and MTL data at equivalent depths. Uncertainty in the CTD measurements are estimated to be 0.01 °C which thus defines a basic uncertainty of the MTL data prior to any additional adjustments applied in subsequent processing steps.

Temperature measurements within a MeBo-borehole are affected by the small length of the MTL (the tip of the probe inserted into the sediment is 15.5 cm long) and by the time required to deploy the tool during which the bottom of the borehole is cooled by the drilling fluid (bottom seawater). The initial sediment in-situ temperatures are therefore in general too cold (Riedel et al., 2018). The magnitude of the temperature difference to the true in-situ condition scales linearly with the temperature difference between bottom water (temperature of the drilling fluid) and in-situ sediment temperature as well as the time of exposure of the borehole prior to temperature measurements. For a temperature difference of 1 °C, the suppression of the measured temperature in the sediment at 5 cm insertion depth of the MTL is 0.06 °C after an exposure of the borehole of 60 minutes. If the MTL tool is inserted by the maximum length of 15 cm, the suppression is only 0.01 °C. In our case study at the Danube deep-sea fan, bottom water temperatures are ~9 °C and the difference to the deepest measurement point is ~3.5 °C. Temperature measurements were conducted with borehole exposure times of ~30 – 90 minutes. We added a correction factor that incorporates the effects of exposure-time, drill-depth, and probe-insertion length to the initially defined equilibrium temperature to estimate the in-situ temperature (Table S1). The total uncertainty in the temperature measurements was estimated to be the sum of the sensor-accuracy after calibration with CTD data and the required adjustment-value applied. A depth-uncertainty of 5 cm was applied to account for possible error in the estimation of how far the MTL was inserted into the sediment. With these uncertainty values, we performed a total-least-squares linear regression (Krystek and Anton, 2007) to the temperature data to estimate a thermal gradient including the standard deviation and 95% confidence intervals.

The in-situ temperatures are then combined with the gas chemistry (Pape et al., 2020) and pore water salinity to estimate the methane hydrate phase boundary and BGHSZ (Tishchenko et al., 2005). Afterwards, we compare that with the depth of the seismically observed BSRs. The conversion of pressure (Pa) to meter below seafloor was done by incorporating sea-water density of the water column (1017 kg/m^3) and sediment pore water (1005 kg/m^3). Also, due to the way how dissociation pressure is determined in the phase boundary by Tishchenko et al. (2005), the conversion requires to account for the average atmospheric pressure (~100 kPa) to be added to the hydrostatic pressure values of seafloor and BSR depths before identifying the crossing point of the temperature-depth-profiles with the phase boundary. Conversion of depth (m) to seismic two-way travel time (s) was achieved with an average P-wave velocity for the water column (~1475 m/s) from acoustic measurements carried out for calibrating multibeam measurements (Bohrmann et al., 2018) and a sub-seafloor velocity-depth function that match the P-wave velocity data from borehole-logging (Riedel et al., 2020). All seismic data were adjusted to the same water-depth datum at intersection points so that the seismically defined seafloor depths match the water depths at the two drill sites.

2.2 Analyses of pore fluid constituents

Sediment from the MeBo and gravity cores was subsampled for pore water analyses (Bohrmann et al., 2018). The pore water was extracted in the ship's cold room at temperatures of

~9 °C (equivalent to the bottom water temperature) with a low pressure-squeezer (3–7 bar). Pore water was filtered through 0.2 µm cellulose acetate Whatman filters and collected in recipient vessels. Onboard measurements included analysis for content of NH_4^+, total alkalinity (TA), and dissolved SO_4^{2-}, Br^-, and Cl^- ions. The respective chemical analytics follow standard procedures (Grasshoff et al., 1999). The pore water content of Cl^-, Br^-, and SO_4^{2-} was determined by ion chromatography using the IAPSO seawater standard for calibration. Chlorinity values in mM were transferred to salinity. In the following, we report salinity using the Practical Salinity Unit (PSU). All MeBo drill core sediments are affected by some infiltration of bottom water, which was used as drilling fluid. Since the pore water is depleted of SO_4^{2-} at depths below 7 mbsf, the measured content of SO_4^{2-} was used to correct for the bottom water contamination, according to the following equation:

$$C_{corr} = (C_{meas} - f_{BW} * C_{BW}) / (1 - f_{BW})$$

where $f_{BW} = SO_{4,meas} / SO_{4,BW}$ is the fraction of bottom water contaminating the pore water sample based on the ratio of the measured sulfate-concentration in the sample and the bottom water, C_{meas} and C_{BW} are the measured concentrations of Cl^-, Br^-, NH_4^+, and TA in the sample and the bottom water, respectively. Bottom water concentrations were determined from bottom water sampled (Bohrmann et al., 2018).

2.3 Seismic data

Several types of seismic data are available for our study region. During expedition MSM34 (RV MARIA S. MERIAN, 2013/2014, Bialas et al., 2014) a set of regional multichannel seismic (MCS) lines were acquired using a single GI gun (volume ~4L, 250 in^3) and a 1050 m long streamer consisting of 168 channels. Additional high-resolution MCS lines were acquired around the horse-shoe shaped slope failure the with a short streamer (237.5 m active length, 76 channels) and small GI gun (volume 1.5 L, 90 in^3). Processing of all the MCS data included geometry definition, sorting, band-pass filtering (10 – 150 Hz) and velocity analyses with normal move-out correction for an initial stack. Time and depth migration were performed using the velocities from the regional MCS-lines. A 3D seismic data volume covering an area of 3.3 × 8.7 km^2 was acquired with the P-Cable system and a single GI gun (volume ~1.5 L, 90 in^3) during expedition MSM34 focusing on the horse-shoe shaped slope failure area (Hillman et al., 2018a). The P-Cable 3D data also cover the drill sites MeBo-17 and MeBo-19. P-cable processing includes 3D bin-sorting and stacking, band-pass filtering (50 – 200 Hz), and time-migration based on interpolated velocity values from the regional MCS data.

3 Results

3.1 In-situ temperature

Seafloor temperature at the MeBo-17 drill site was defined as average value from the miniature temperature data logger (MTL) used with MeBo200 when the MTL was stored inside the rig in between individual deployments and confirmed by deployments with the thermal heat-probe (Bohrmann et al., 2018). These values are in good agreement with water column temperature measurements conducted during various previous expeditions (Bialas et al., 2014; Riboulot et al., 2018; Bohrmann et al., 2018). Adjustment values to the MTL-based downhole temperature measurements are required to account for cooling effects by the borehole fluid (Riedel et al., 2018). The adjustments vary from a minimum of 0.018 °C (at 7.35 mbsf) to a maximum of 0.051 °C (at 143.85 mbsf). The adjusted temperature values (Table S1) then suggest an average thermal gradient of 21.86 (±0.3) °C/km over the drilled sediment interval excluding the seafloor data point. If the seafloor temperature is included but not fixed, the best-fit gradient is ~23.78 (±0.24) °C/km. A seafloor intercept of the linear gradient is calculated to 9.02 (±0.01) °C. Temperature readings in the shallow-most sediments can be affected by temperature variations in the water column (Hillman et al., 2018a) as noted from deployments with a 6m-long heat-probe around the MeBo200 drill sites. As a result, estimated temperature gradients can be too high (Bohrmann et al., 2018). We use an average thermal gradient of 23.78 (±0.24) °C/km to best describe the results from the MeBo200 drilling if a linear gradient is to be used.

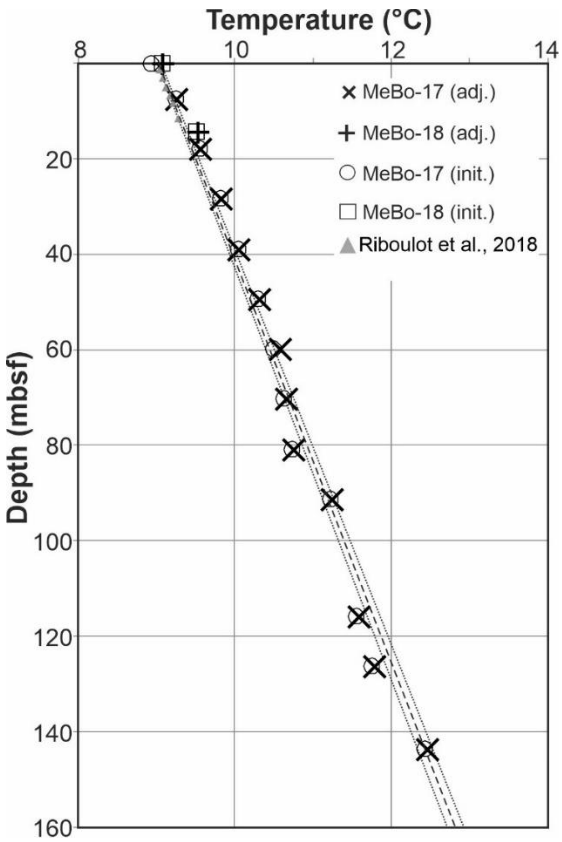

Figure 2 (a) Downhole temperatures derived at Site MeBo-17 and MeBo-18 (Table 1). These data suggest an average thermal gradient of 23.78 (±0.24) °C/km (dashed black line is the average thermal gradient with two standard deviations (equivalent to a 95% confidence interval) shown as dotted lines). Also included are the initial temperature values (open symbols) before adjustment (crosses). For comparison, temperature data up to 12 m below seafloor from station CSF4 (Calypso Flux coring system, GHASS Expedition with R/V *Pourquoi pas?*; Riboulot et al., 2018), ~2.8 km east of MeBo-16, are also shown.

<u>3.2 Pore fluid constituents and sediment physical properties</u>

At all MeBo drilling sites, the uppermost 25 mbsf of sediments are characterized by a steep decline in pore fluid salinity from bottom water values of ~22 PSU to nearly constant values around 2 – 3 PSU for the remainder of the bore hole (Figure 3a). This decline is also evident in all gravity and piston cores taken across the region (Soulet et al., 2010) and consistent with observations made during DSDP drilling (Ross et al., 1978) and coring performed during the GHASS expedition (Ker et al., 2019; Riboulot et al., 2018). Sediment porosity shows a steep decrease in the upper 25 mbsf from 0.9 to 0.5 and (with small variation) remains nearly constant below at values around 0.4 to 0.5 (Figure 3b). The sediment column drilled with MeBo200 is mostly comprised of uniform sediments consisting of clay to silty clay (Bohrmann et al., 2018) with only subtle variation below 40 mbsf as shown by the natural gamma-ray log (Figure 3c). P-wave velocity (Figure 3d) and bulk density (Figure 3e) overall show also little changes yielding small impedance contrasts overall associated with a low-amplitude seismic reflection character (Figure S3) (Riedel et al., 2020).

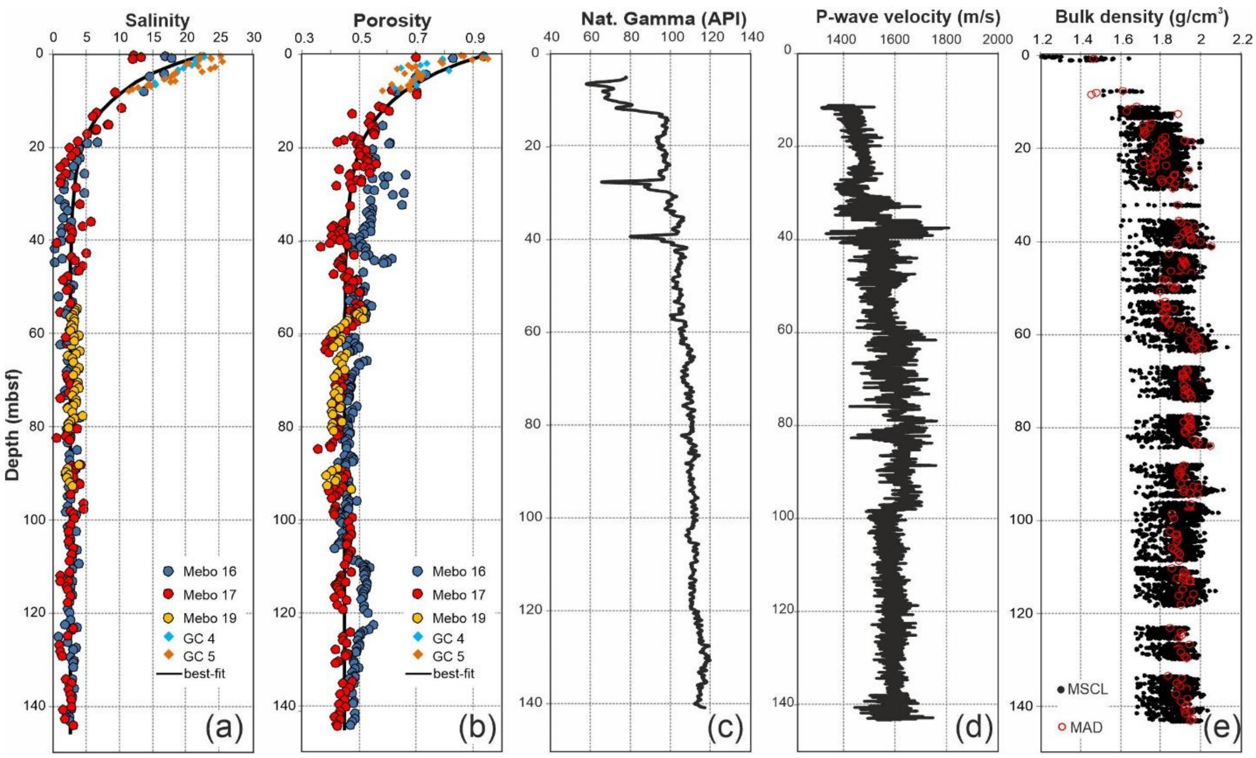

Figure 3 Depth profiles of (a) pore fluid salinity, and (b) porosity from all MeBo drill sites and coincident gravity cores (GC). A steep decline in salinity from near-seafloor values of ~22 PSU to almost constant values around 3 at greater depth is evident. Also shown are (c) natural gamma-ray and (d) P-wave velocity log-data acquired at Site MeBo-17 and (e) bulk density record obtained post-drilling from cores taken at Site MeBo-17.

<u>3.3 Seismic data and BSRs</u>

As shown in Figures 4, a prominent reflection, called BSR-1, is identified in the MCS data crossing the stratigraphy and showing a polarity opposite to that of the seafloor reflection. This has been interpreted as the current expression of the sI BGHSZ (Popescu et al., 2006; Zander et al., 2017, Hillman et al., 2018a). Below this reflection, up to two additional BSRs are identified at MeBo-16, and following nomenclature previously introduced (Zander et al., 2017) those are BSR-2 and BSR-3. We mark these events on MCS lines 897-03 and 897-15 in Area-1 near the MeBo sites of the S2 channel (Figure 4a, b). We also created a splice through the drill sites using the available seismic data (Figure S3) highlighting the continuous levee-stratigraphy in the region (Riedel et al., 2020). The higher-frequency P-Cable 3D data (Figure 4c, S4a) and high-frequency 2D line P4105 (Figure S4b) also clearly show BSR-1. In Area 2 around the S4 channel, the BSR-1 is identified along MCS lines 897-04 (Figure 4d), 897-24 (Figure S5a), and 897-05 (Figure S5b). Along the seismic lines strong seismic reflection amplitude cut-offs appear shallower than BSR-1 and when connected, they mimic a BSR-like behaviour. In some instances, a continuous reflection, cross-cutting, and of opposite polarity to the seafloor is fully developed within the P-Cable 3D data (Figure 4c) and some of the 2D MCS data (Figure 4a, d). This shallower BSR-like event is called BSR-0 for discussion purposes and marked in orange on the seismic sections. We also present a collage of close-up images of these BSR-0 events in Figures 4e-g.

Within the 3D data at the S2 channel, several bright spots developed above BSR-1 along the western levee, SW of the MeBo-17/-19 drill sites (Figure 5a). The bright spots are tied to a specific horizon (Horizon-A) which was traced through the 3D data. The reflection of this horizon is mostly dim but polarity is opposite to that of the seafloor indicating a density reversal (Riedel et al., 2020). We extracted seismic amplitude and similarity attributes along horizon-A revealing a consistent fault pattern (Figures 5c). The occurrence of the bright spots is tied to the fault pattern depicted by the 3D data (Figure 5d). Above Horizon A, another polarity reversed reflection is seen that does not exhibit any bright spots although the same faults tied to the bright spots below are cutting through this reflection. Below BSR-1, reflection amplitude of all layers is much increased and the dip of the layers within the levee complex is generally towards the SE.

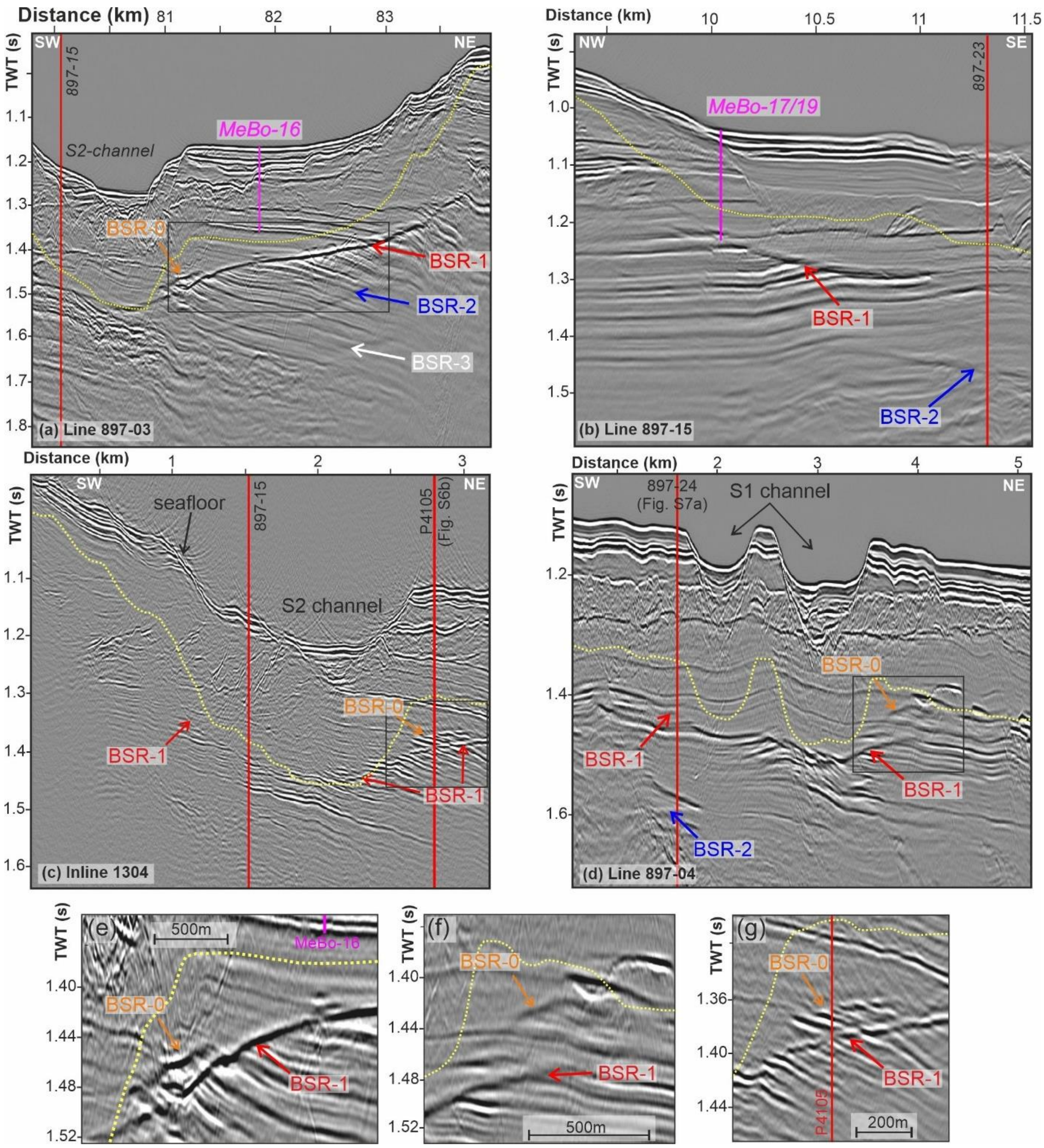

Figure 4. Images of 2D seismic data showing multiple BSRs in the Danube deep sea fan region. Examples from the S2-channel: (a) line 897-03 (MeBo-16), (b) line 897-15 (MeBo-17), and (c) inline 1304 (P-Cable). Example from the S4-channel: (d) line 897-04. Location of lines see Figure 1. Yellow dotted line is base of gas hydrate stability (1D model) given today's conditions based on MeBo drilling (seabed temperature of 9°C, thermal gradient of 23.78 °C/km). Images of (e) - (g) are close-ups of boxes shown in (a) – (d) highlighting BSR-0 above BSR-1.

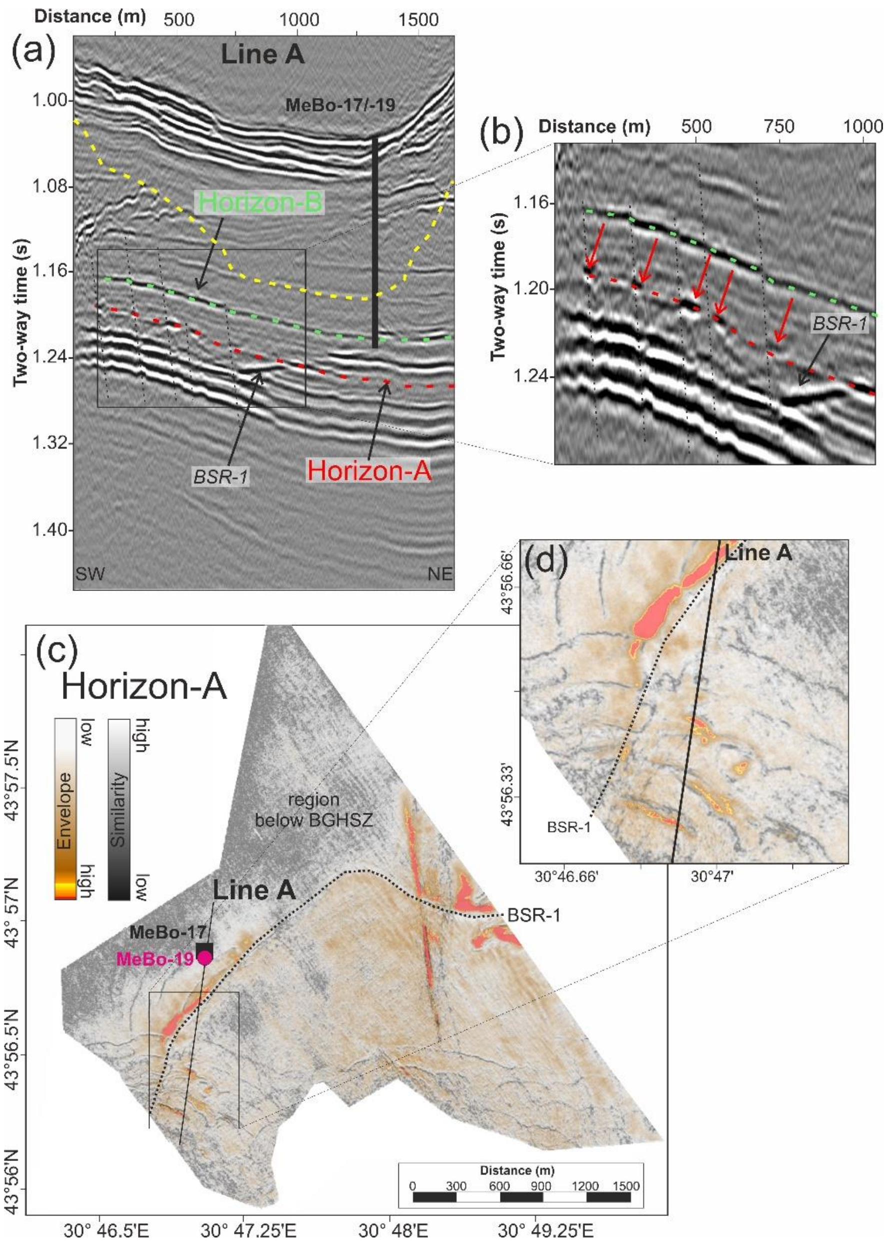

Figure 5. Section from 3D P-Cable data (Line A) through MeBo-17/-19 drill sites showing bright spots at fault intersections (thin dashed lines indicate faults), highlighted in close-up view (b) with red arrows. The bright spots are an indication of vertical gas migration. Yellow dashed line is the estimated current base of the gas hydrate stability zone (seabed temperature of 9°C, thermal gradient of 23.8 °C/km). Note, the faults penetrate also Horizon B (green dashed line) but no bright spots develop at this horizon. (c) Map of Horizon-A with attributes of reflection strength and similarity combined. (d) close-up map of region of bright-spots identified in (b). Intersection of BSR-1 with horizon is shown as dotted line.

4 Discussion and Interpretation

The new drilling data down to ~144 mbsf acquired during expedition M142 allows a detailed interpretation of the dynamic gas hydrate system in the deep-sea fan of the western Black Sea as critical in-situ observations were missing before (Riboulot et al., 2018; Ker et al., 2019). Since the LGM, bottom water temperature in the Black sea is increasing and sea-level has risen by ~100 m. Those processes resulted in an effective upward shift of the BGHSZ (Riboulot et al., 2018; Ker et al., 2019) as the large increase in temperature (upward shift) overwhelms the opposite effect from the increase in hydrostatic pressure (downward shift). Previous work has shown wide-spread BSRs in the slope region of the Danube deep sea fan, including up to 4 paleo-BSRs attributed to various former climate stages with stable temperature and pressure conditions (Popescu et al., 2006; Zander et al., 2017). The prominent seismic reflection identified as BSR-1 in previous studies (Baristeas, 2006; Popescu et al., 2006, 2007) was initially attributed to today's climate conditions. Subsequent modelling showed that this may not be necessarily correct (e.g. Hillman et al., 2018b; Zander et al., 2017; Ker et al., 2019) but deep borehole data were lacking. Our new temperature and borehole data from the MeBo drilling during M142 confirm that the BSR-1 is not marking the current BGHSZ in the western Black Sea as outlined below.

4.1 Downhole temperatures

Previous work in the Black Sea on thermal gradients and modelling of the gas hydrate stability zone were performed based on heat-probe systems with sediment-penetration depths of typically 6 m (Vasilev, 2015; Hillman et al., 2018b) or using thermal probes mounted on the outside of coring devices (Römer et al., 2020; Riboulot et al., 2018). These shallow penetration systems result in thermal gradients that may not be representative for the deeper sediment section, especially at BSR depths >140 mbsf, particularly in dynamic, thermally not equilibrated systems as the Black Sea. The new temperature information from MeBo drilling allows to address changes in the thermal state of the upper 100 m – 200 m of sediments below seafloor induced since the end of the LGM, and to correct for errors involved in projecting a linear gradient from heat-probe data to BSR depths. As seen at Site MeBo-17 (Figure 2), down-hole temperatures deviate from a linear trend over the shallowest portions of the borehole up to ~30 mbsf with a slight concave pattern that reflects the decline in porosity and associated change in thermal conductivity. Within the uncertainty limits of the MeBo temperature data, we do not observe a temperature-depth profile that reflects the impact of bottom-water warming since the LGM (i.e. a convex-shaped profile) as e.g. shown in the model by Zander et al., (2017). Thus, the warming-process of the sediments over the depth interval cored may have already reached a near temperature-equilibrium, which is similar to the findings described by Ker et al. (2019). Therefore, using a linear thermal gradient may be (within the limits of all uncertainties) applicable for a first-order estimate of the BGHSZ and discussion on its depth relative to seismically inferred BSRs.

4.2 Depth of the base of gas hydrate stability zone

Using the temperature data and core-derived properties of pore water salinity and gas molecular composition allows calculating the phase boundary for sI methane hydrate at the drill sites (Figure 6). At Site MeBo-17, the pore water salinity for the depths below 40 mbsf is 2 – 3 PSU (Figure 3). The temperature data from all tool deployments determine an average thermal gradient of ~23.78 (±0.24) °C/km, which intersects the sI methane hydrate phase boundary for a salinity of 3 PSU at ~110.5 mbsf (Figure 6a). However, uncertainties in the thermal gradient and fluctuations in pore water salinity (Figure 3a) define an interval for the possible BGHSZ (Figure 6). The method of total-least-squares applied in the linear regression incorporates all measurement uncertainty in depth and temperature and is superior to simple linear regression due to the depth-dependent uncertainty in the temperature-adjustment needed to account for the bore-hole cooling prior to the measurement itself. Using a salinity of 2 PSU and a lower thermal gradient of 23.3 °C/km then results in a BGHSZ at 118 mbsf. In contrast, using a higher salinity of 3 PSU and a steeper thermal gradient (24.26 °C/km) results in a BGHSZ at 106 mbsf.

At Site MeBo-16, no in-situ temperature data exist but pore water data suggest a similar range in salinity values at depths below ~40 mbsf. We use the geothermal gradient defined from

MeBo-17 to estimate the BGHSZ (Figure 6c, d) for a bottom water temperature of 9.01 (±0.01) °C from the coincident heat-probe deployment (Bohrmann et al., 2018). Using the same range in parameters yields a 95% confidence interval for the BGHSZ ranging from 165 mbsf (3 PSU, 24.26 °C/km) to 179 mbsf (2 PSU, 23.3 °C/km). An average value for the BGHSZ at MeBo-16 is thus 172 ±7 mbsf.

As expected, the pore-fluid salinity in the sediments below 40 mbsf is lower than that of current bottom seawater (~22 PSU, e.g. Öszoy and Ünlüata, 1997) reflecting the depositional environment when the Black Sea was a fresh-water lake (Ross et al., 1978; Soulet et al., 2010; Constantinescu et al., 2015)). The smooth pore water salinity profile determined at the MeBo drill sites reflects the current balance between upward diffusion of salt from deeper sections with higher salinity reflecting the hyper-saline stage of the Black Sea (e.g. Calvert and Batchelor, 1978; Manheim and Schug, 1978) into the fresh-water interval of the last glacial period, and the downward diffusion of salt from current bottom waters. Another process to reduce the pore water salinity upon core-recovery is the dissociation of gas hydrates (e.g. Hesse, 2003). In open-ocean environments when sediments were deposited in an always-saline environment, the deflection of pore water salinity to lower than the background level (e.g. a salinity of 34 PSU) has successfully been used to infer the presence and concentration of gas hydrates (e.g. Kastner et al., 1995; Torres et al., 2004). Thus, if gas hydrates were present in the sediments at the MeBo drill sites, their dissociation prior to the pore water sampling could locally depress the pore water salinity further. During the processing of MeBo cores and prior to pore water sampling, infra-red (IR) imaging was used to infer the presence of gas hydrates (Bohrmann et al., 2018). However, no cold-spot anomalies were recognized in the IR data, probably a result of overall low in-situ gas hydrate saturations and damping of any temperature signal from gas hydrate dissociation due to a long time-span of usually ~1 hr between the time the cores were outside the gas hydrate stability zone (upon MeBo200 recovery at water depths ~400 m), core recovery from the magazines, and final IR imaging on deck. Cross-plots of $\delta^{18}O$-$\delta^{2}H$ of the porewater at sites MeBo-16 and MeBo-17

(Pape et al., 2020) show that the pore water data lie overall on a local meteoric water line, suggesting no significant gas hydrate presence in the recovered sediments. At Site MeBo-16, previous velocity-based inferred gas hydrate saturations for the depth interval cored are ~5% of the pore space (Ker et al., 2019), generally in agreement with our borehole-based observations.

Core-log-seismic integration (Riedel et al., 2020) and prior MCS velocity analyses (Zander et al., 2017) did show that P-wave velocity is well constrained with only minor uncertainty. On average, P-wave velocity from MCS data is 1600 m/s for the interval from seafloor to BSR. The P-wave log from site MeBo-17 (Figure 3d) also confirms this as an average value. Upper and lower bounds in velocity were defined yielding a range in velocity from 1560 to 1640 m/s. Together with a small uncertainty in defining the BSR and seafloor two-way travel-times on seismic sections (2 ms), this results in a small uncertainty in the BSR-1 depth values. Time-depth conversion yields a BSR-1 depth at Site MeBo-17 of ~144 ±4 mbsf. Here, additional evidence for free gas at this depth came from visual observation of gas bubbles rising through the drill string to the seafloor (Figure S6) observed with the bottom-cameras attached to the MeBo rig (Bohrmann et al., 2018). The BSR-1 at Site MeBo-16 is at ~202 ±5 mbsf, accordingly. Overall, the estimated intervals for the current BGHSZ based on a linear thermal gradient and the BSR-1 depths are not matching at the MeBo-16 and MeBo17/19 drill sites, and the current BGHSZ is always significantly shallower than the BSR-1 (Figure 6).

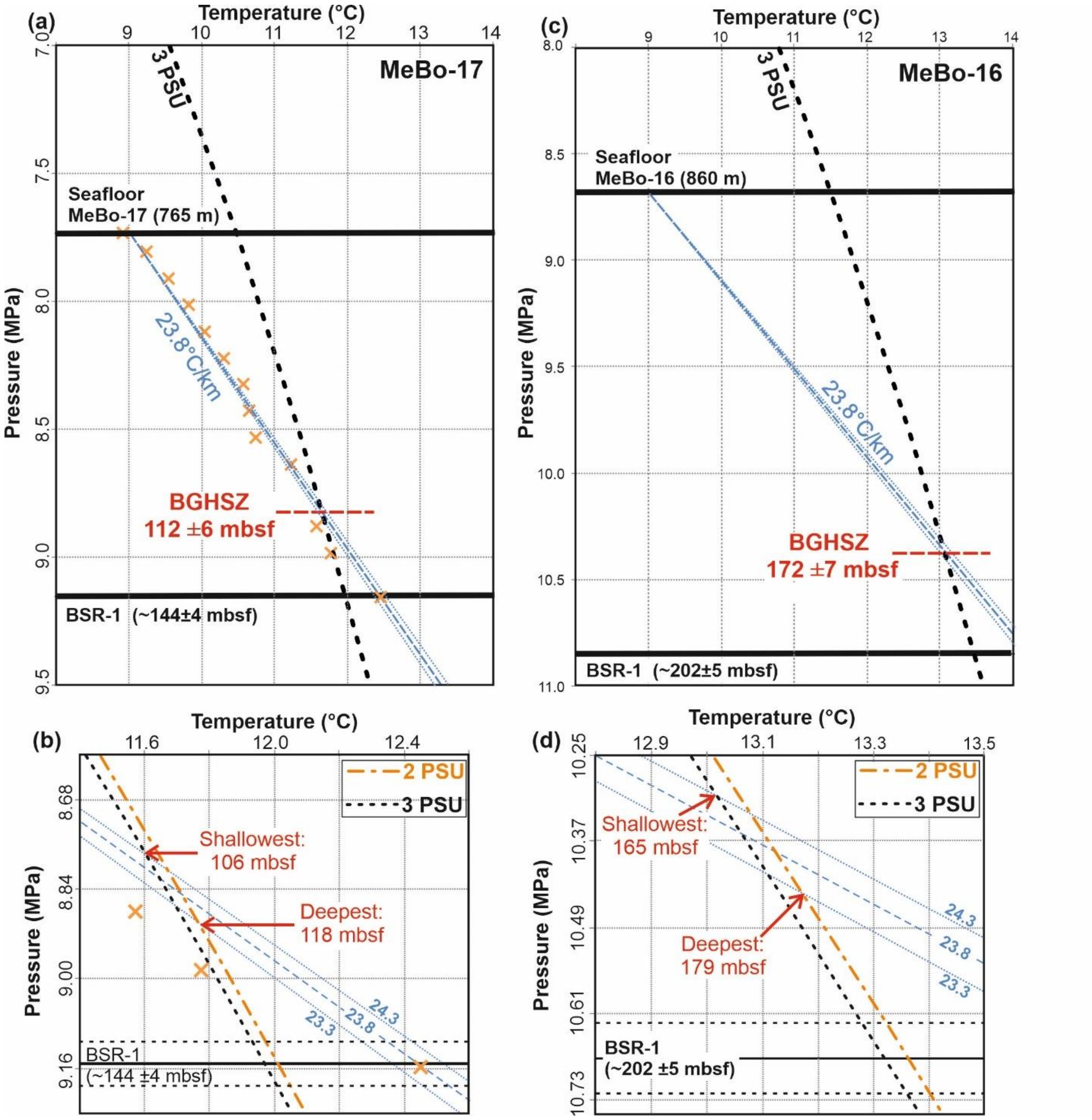

Figure 6. Calculation of structure I gas hydrate phase stability zone (BGHSZ) at MeBo-17 (a, b) and MeBo-16 (c, d). Geothermal gradients are shown for an average value of 23.78 °C/km as well as upper and lower bounds of the 95% confidence intervals. Upper and lower limits in the crossing points of geothermal gradients with the sI gas hydrate phase boundaries for salinities of 2 and 3 PSU define the interval for the estimated BGHSZ. Note, labels of values in Figure are rounded to one decimal. In-situ measurements (orange crosses) are shown at Site MeBo-17. The BGHSZ at MeBo-17 is estimated at ~112 ±6 mbsf, shallower than the BSR-1 (~144 ±4 mbsf). At Site MeBo-16, the BSR was identified at ~202 ±5 mbsf. Here, the BGHSZ is at ~172 ±7 mbsf.

4.3 Seismic observations of multiple BSRs

The deepest temperature measurement at Site MeBo-17 at 143.85 mbsf is clearly within the realm of free gas (temperature higher than what is required for solid hydrate, Figure 6a, b) even for the smallest in-situ salinity assumed. The measurement at a depth of 126.35 mbsf is situated just at the edge of the phase boundary (see Figure 6a, b), which is slightly deeper than the crossing point of the phase boundary with the assumed average linear temperature gradient (which was at 125.5 ±10 mbsf). Thus, the current temperature conditions indicate that the BGHSZ is significantly shallower than the BSR-1, even when taking all uncertainties and limits of the method involved into account. The shallow BSR-0 seen above the BSR-1 (Figures 4, 5, S4, S5) could therefore be the result of the new thermal conditions imposed since the LGM. The depth-difference between BSR-0 and BSR-1 (~15 m) is about the same as the difference between the modelled current BGHSZ and BSR-1 at the drill sites MeBo16 and MeBo-17. This BSR-0 is seen most prominently along the eastern levees of the S2 and S4 channels. We also observe from the distribution of the various BSRs, that the relic BSR-2 and the shallow BSR-0 do not overlap regionally, which also is true for the region of fault-promoted vertical gas flow (Figure 7).

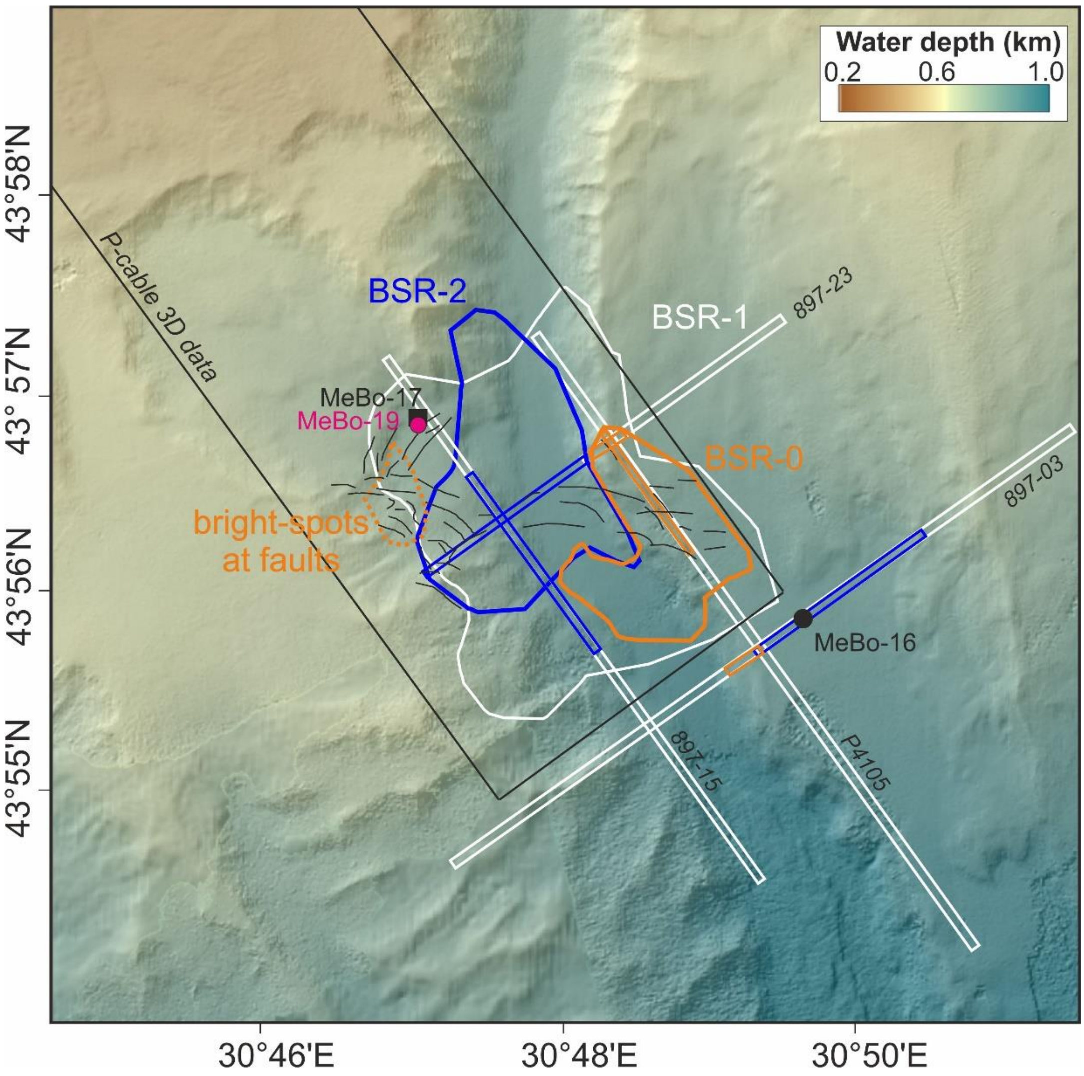

Figure 7 Map of distribution of various BSRs observed in the region of the MeBo drilling sites at the S2 channel (Area 1). BSR-1 is shown in white outline, BSR-2 in blue, and BSR-0 in orange. Superimposed on the bathymetry are the fault patterns of the horizon shown in Figure 5.

Zander et al. (2017) showed that former BGHSZs (seismically seen as multiple BSRs) can survive for prolonged periods in time as seismic expression of the presence of free gas. Formation of a laterally continuous BSR requires stable climate conditions so that sufficient free gas can accumulate at the stationary phase boundary to produce a sufficient acoustic impedance contrast. Local permeability barriers are required for hampering free gas migration and solubility of methane must also be a limiting factor; otherwise, gas would be dissolved and no seismic reflection can occur from the impedance contrast between gas-free and gas-bearing sediments. Where gas could migrate laterally or vertically, the paleo-BSRs may no longer be seismically identified. This explains the pattern of multiple BSRs at the S2 channel (Figures 7). Where the BSR-2 disappears, a BSR-1 and BSR-0 are seen, highlighting gas migration along strata as well as faults. The (small) region of bright spots developed SW of the MeBo-17/-19 drill sites also show the characteristics of a BSR-like pattern if the bright-spots are connected (Figure 5a, b). The gas migrated along the faults vertically until it reached a suitable host-strata where the free gas amplifies the reflection strength. The Horizon A which shows the bright spots is still deeper than the predicted BGHSZ using 1D modelling (Figure 5). The faults seen continue to shallower depth (to ~100 mbsf) but do not reach all the way to the seafloor. Yet, a prominent reflection above Horizon A that is also cut by the faults does not exhibit any bright spots.

The occurrence of a BSR-0 across the eastern levee region of the S4 channel is observed only at a few MCS lines but a laterally continuous BSR-1 and BSR-2 are seen. The modelled BGHSZ for current conditions (bottom water temperature of 9 °C) is shallower than BSR-1 but a thermal gradient of 23.78 °C/km determined at MeBo-17 may not be as applicable at the S4 channel due to the distance between the sites (~25 km). However, pore water salinity conditions should be similar between those two regions given the nature of the mostly layered levee-sediments and their similar sub-seafloor depth. As we only have few seismic lines available around the S4 channel, interpretation of the short BSR-0 segments are uncertain. However, the similarities between the S2- and S4-channels are striking.

The current BGHSZ (BSR-0) has for most regions in the study area no seismic expression of a free gas layer underneath the phase boundary (with the few exceptions shown), which has several implications: (i) Gas hydrate was not present in the sediment above BSR-1 as otherwise we would see a free gas reflection from dissociated gas hydrates or a BSR-like event from the contrast in hydrate-bearing sediment above hydrate-free sediments below the current depths of the BGHSZ. (ii) Methane from gas hydrate present in the past is fully dissolved into the pore water, so no excess free gas exists to form a seismic expression of a new BSR-0. Thus, former gas hydrate concentrations must have been overall low to allow for such a process to work. (iii) Gas migration and sediment permeability (on the pore scale along layers and on a macroscopic scale involving faults or fractures) must be mostly low in the depth interval around BSR-1 with free gas remaining at the paleo-depth corresponding to former stable gas hydrate conditions.

4.4 Implications

The borehole temperature data suggest a BGHSZ that is 15 – 20 m shallower than what is seismically imaged as the BSR-1 (Figure 6). In several regions a 'new' BSR-0 has developed at shallower depths (Figures 4, S4, S5). The depth difference between BSR-1 and BSR-0 is at most ~20 m and is best seen on the eastern wall of the levees of the S2 and S4 channels. The seismic reflection of the BSR-0 is seen systematically in all different seismic data types available in the study region. We suggest that the adjustment within the sediment system from the LGM to the present-day conditions is still ongoing, resulting in a still changing gas hydrate stability zone. The BGHSZ has moved upwards to shallower levels but free gas migration from greater depth (where it was trapped at the BSR-1) has not kept up with the faster temperature adjustments on a regional scale. However, gas migration occurs laterally along more permeable strata and is locally promoted through faulting resulting in a new, but patchy free-gas reflection that is mimicking BSR-type behaviour. Based on simple 1D diffusion modelling we infer a first-order estimate of the time required for methane to diffuse upwards towards the newly established BGHSZ from the BSR-1 depths. Assuming an effective methane diffusivity of ~4.5×10^{-10} m^2/s in pore water (salinity of 3, temperature of 10°C, pressure of 10 MPa, porosity of 0.45, following Kossel et al., 2013) it would require ~8,000 years for methane to diffuse upwards over a distance of 15 m. This is approximately the same time span since the connection between Black Sea and Mediterranean Sea was re-established (e.g. Soulet et al., 2011). Since the BSR-1 still lags behind the shallower BGHSZ, gas migration (either by diffusion or as free gas bubbles) must be more severely slowed down. This could be linked to pore-throat effects limiting the ascent of free gas bubbles by pure buoyancy (Schowalter, 1979), or capillary effects that locally impact methane solubility (Liu and Flemings, 2011). Alternatively, Ker et al. (2019) argued that initial gas hydrate dissociation due to the (faster) thermal equilibration resulted in some amount of over-pressure (free gas from dissociation cannot quickly dissipate), which in turn enables re-formation of gas hydrate below the current steady-state BGHSZ (assuming hydro-static pressure) and above the former BSR-1. Our new drilling at MeBo-16 and MeBo-17/19 did show no evidence for the presence of any significant gas hydrate from coring or geophysical logging in the depth interval above the BSR-1 where this re-formed gas hydrate would be located. In particular, the P-wave velocity log at MeBo-17 (Figure 3d) shows nearly no variation at all around an average value of 1600 m/s that may be from gas hydrates, thus arguing against the hypothesis by Ker et al. (2019) of over-pressure-related re-formation of hydrates.

In general, this new study and previous work in the Black Sea highlight the complexities and limitations involved in relating seismically observed BSRs to the gas hydrate stability zone and a thermal regime. The assumption of linear gradients may not uniformly apply, especially in regions with strong post-glacial temperature and pressure changes such as the Black Sea or Arctic margins, or regions with recent tectonic events or slope failures. Discrepancies between theoretical predictions of the BGHSZ and seismically observed BSRs have been observed along several other continental margins e.g. off Svalbard by Plaza-Faverola et al. (2017) or the Blake Ridge off the eastern US Atlantic margin by Ruppel (1997). The observed differences may be related to capillary effects on the methane solubility (Liu and Flemings, 2011) or complex mixes of hydrocarbons (other than methane). These studies all highlight the need for high-quality in-situ temperature measurements, a suite of sediment physical properties useful for thermal modelling (i.e. porosity and/or thermal conductivity), and a good control on seismic velocity (from logging data or MCS data) to reduce uncertainties in the time-depth-conversion.

5 Conclusions

The wealth of new drilling data especially temperature down to ~144 mbsf acquired during expedition M142 allowed a detailed new interpretation of the dynamic gas hydrate system in the Danube deep-sea fan of the western Black Sea. Since the last glacial maximum (LGM), bottom water temperature in the Black sea is increasing and sea-level has risen by ~100 m. This combination will shift the base of the gas hydrate stability (BGHSZ) upwards. Previous work has shown wide-spread BSRs in the slope region of the Danube deep sea fan, including up to 4 paleo-BSRs attributed to various former climate stages with stable temperature and pressure conditions. The prominent seismic reflection identified as BSR by previous researchers was attributed to today's climate conditions. However, our new work showed that this is not necessarily the case in the western Black Sea. The borehole temperature data suggest on average a BGHSZ ~20 m shallower than what is seismically imaged as the BSR (here called BSR-1). In several regions a 'new' BSR has developed (here called BSR-0) above the BSR-1. The depth difference between BSR-1 and BSR-0 is ~15 m and is best seen on the eastern wall of the levees of the S2 and S4 channels. The seismic reflection of the BSR-0 is seen systematically in all different seismic data types available in the study region. We conclude that the adjustment of the sediment-temperature conditions imposed since the LGM may have reached a near equilibrium and established a shallower gas hydrate stability zone than expected from BSR depths. Yet, gas migration lags behind and gas is still moving upwards to shallower levels establishing a new BSR over time. Gas migration from greater depth where it was formerly trapped at the BSR-1 occurs laterally along more permeable strata but is also locally promoted through faulting. Using the BSR as proxy for geothermal gradients may be misleading and should be treated with caution especially in the absence of any deep drilling data.

Acknowledgments

The authors would like to thank all ship-crews, support staff, and scientific personnel involved in conducting on board work and analyses during expeditions MSM34 and M142. R/V METEOR cruise M142 and R/V MARIA S. MERIAN cruise MSM34 were fully integrated into the German collaborative gas hydrate program SUGAR, which also provided the funding for scientific work of the cruise (BMWi 03SX20A+G & 03SX381F, BMBF 03G0819A & 03G0856A). Cruise MSM34 was further supported by project MIDAS (EU-FP7 grant 603418).

.

Data Availability

Seafloor bathymetric data shown are available at the Pangaea data repository: https://doi.pangaea.de/10.1594/PANGAEA.895506. All seismic data used in this study are also available for download at the Pangaea data base. The 3D data can be accessed here: https://doi.org/10.1594/PANGAEA.921631. The 2D seismic sections can be accessed here: https://doi.org/10.1594/PANGAEA.921576. Raw temperature records from the miniature temperature loggers (MTL) used to measure temperature in-situ downhole are shown in the Supplementary information and can be accessed at the Pangaea repository at: https://doi.pangaea.de/10.1594/PANGAEA.921715.

References

Baristeas, N., 2006. Seismische Fazies, Tektonik und Gashydratvorkommen im nordwestlichen Schwarzen Meer, Diploma Thesis, University Hamburg, p. 110.

Bialas, J., Klaucke, I., Haeckel, M., 2014. FS MARIA S. MERIAN Fahrtbericht / Cruise Report MSM-34 / 1 & 2 – SUGAR Site, GEOMAR Report, No. 15, GEOMAR Helmholtz Centre for Ocean Research Kiel, Kiel, 109 pages, doi:10.3289/GEOMAR_REP_NS_15_2014.

Bohrmann, G., Ivanov, M., Foucher, J.P., Spieß, V., Bialas, J., Weinrebe, W.R., Abegg, F., Aloisi, G., Artemov, Y.G., Blinova, V.N., Drews, M., Greinert, J., Heidersdorf, F., Krastel, S., Krabbenhöft, A., Polikarpov, I.G., Saburova, M., Schmale, O., Seifert, R., Volkonskaya, A., Zillmer, M., 2003. Mud volcanoes and gas hydrates in the Black Sea - new data from Dvurechenskii and Odessa mud volcanoes, Geo-Marine Letters, 23(3-4). 239-249. doi:10.1007/s00367-003-0157-7

Bohrmann, G., and 47 other authors, 2018. R/V METEOR cruise report M142, Drilling Gas Hydrates in the Danube Deep-Sea Fan, Black Sea, Varna – Varna – Varna, 04 November – 22 November – 09 December 2017. Berichte, MARUM – Zentrum für Marine Umweltwissenschaften, Fachbereich Geowissenschaften, Universität Bremen, No. 320, 121 pp., ISSN 2195-9633, http://publications.marum.de/id/eprint/3698.

Calvert, S.E. Batchelor, C.H., 1978. Major and minor element geochemistry of sediments from Hole 379A, Leg 42B, Deep-Sea Drilling Project, Initial Reports of the Deep Sea Drilling Project 42, Part2, 527–541.

Collett, T.S., Johnson, A.H., Knapp, C.C., Boswell, R., 2009. Natural gas hydrate: a review, AAPG Memoir 89, 146-219.

Constantinescu, A., Toucanne, S., Dennielou, B., Jorry, S., Mulder, T., Lericolais, G., 2015. Evolution of the Danube deep-sea fan since the last glacial maximum: new insights into black sea water-level fluctuations, Marine Geology, 367, 50 – 68, https://doi.org/10.1016/j.margeo.2015.05.007.

Freudenthal, T., Wefer, G., 2013. Drilling cores on the sea floor with the remote-controlled sea floor drilling rig MeBo, Geoscientific Instrumentation, Methods and Data Systems, 2(2). 329-337, doi:10.5194/gi-2-329-2013.

Ginsburg, G.D., 1998. Gas hydrate accumulation in deep-water marine sediments. In: Henriet, J.-P. & Mienert, J. (eds) Gas Hydrates: Relevance to World Margin Stability and Climate Change. Geological Society, London, Special Publications, 137, 51-62, available online: https://sp.lyellcollection.org/content/specpubgsl/137/1/51.full.pdf, accessed June 25, 2020.

Grasshoff, K., Ehrhardt, M., Kremling, K., 1999. Methods of Seawater Analysis. Wiley-VCH, Weinheim, 632pp.

Greinert, J., McGinnis, D.F., Naudts, L., Linke, P., De Batist, M., 2010. Atmospheric methane flux from bubbling seeps: Spatially extrapolated quantification from a Black Sea shelf area, Journal of Geophysical Research: Oceans, 115, C01002, doi:10.1029/2009JC00538.

Hesse, R., 2003. Pore water anomalies of submarine gas-hydrate zones as tool to assess hydrate abundance and distribution in the subsurface. Earth-science Reviews 61(1-2), 149-179, https://doi.org/10.1016/S0012-8252(02)00117-4.

Hillman, J.I.T., Klaucke, I., Bialas, J., Feldman, H., Drexler, T., Awwiller, D., Atgin, O., Çifçi, G., 2018a. Gas migration pathways and slope failures in the Danube Fan, Black Sea, Marine and Petroleum Geology, 92, 1069-1084, https://doi.org/10.1016/j.marpetgeo.2018.03.025.

Hillman, J.I.T., Burwicz, E., Zander, T., Bialas, J., Klaucke, I., Feldman, H., Drexler, T., Ahrwiller, D., 2018b. Investigating a gas hydrate system in apparent disequilibrium in the Danube Fan, Black Sea, Earth and Planetary Science Letters, 502, 1-11, https://doi.org/10.1016/j.epsl.2018.08.051

Kastner, M., Kvenvolden, K.A., Whiticar, M.J., Camerlenghi, A., Lorenson, T.D., 1995. Relation between pore fluid chemistry and gas hydrates associated with bottom-simulating reflectors at the Cascadia margin, Sites 889 and 892. In Carson, B., Westbrook, G.K., Musgrave, R.J., and Suess, E. (Eds.), Proc. ODP, Sci. Results, 146 (Pt. 1): College Station, TX (Ocean Drilling Program), 175–187. doi:10.2973/odp.proc.sr.146-1.213.1995

Ker, S., Thomas, Y., Riboulot, V.,Sultan, N., Bernard, C., Scalabrin, C.,Ion, G., Marsset, B., 2019. Anomalously deep BSR related to a transient state of the gas hydrate system in the western Black Sea, Geochemistry, Geophysics, Geosystems, 20, 442–459. https://doi.org/10.1029/2018GC007861

Klaucke, I., Sahling, H., Weinrebe, W.Blinova, V., Bürka, D., Lursmanashvili, N., Bohrmann, G., 2006. Acoustic investigation of cold seeps offshore Georgia, eastern Black Sea, Marine Geology, 231(1–4), 51-67, https://doi.org/10.1016/j.margeo.2006.05.011

Kossel, E. Bigalke, N., Piñero, E., Haeckel, M., 2013. The SUGAR Toolbox - A library of numerical algorithms and data for modelling of gas hydrate systems and marine environments. GEOMAR Report (N. Ser.), 8, 160 pp., https://doi.org/10.3289/geomar_rep_ns_8_2013

Krystek, M., Anton, M., 2007. A weighted total least-squares algorithm for fitting a straight line, Measurement Science and Technology, Vol. 18, No. 11, 3348 – 3442

Küçük, H.M., Dondurur, D., Özel, Ö., Sinayuç, Ç., Merey, S., Parlaktuna, M., Çifçi, G., 2015. Gas and Gas Hydrate Potential Offshore Amasra, Bartin and Zonguldak and Possible Agent for Multiple BSR Occurrence, Geophysical Research Abstracts, 17, EGU2015-10310-1, 2015 EGU General Assembly 2015.

Liu, X., Flemings, P.B., 2011. Capillary effects on hydrate stability in marine sediments, Journal of Geophysical Research, 116, B07102. https://doi.org/10.1029/2010JB008143

Manheim, F.T., Schug, D.M., 1978. Interstitial waters of Black Sea cores. In: Initial Re-ports of the Deep Sea Drilling Project, 42 Pt.2. U.S. Government Printing Office, 637–651.

Minshull, T.A., Marín-Moreno, H., Betlem, P., Bialas, J., Buenz, S., Burwicz, E., Cameselle, A.L., Cifci, G., Giustiniani, M., Hillman, J.I.T., Hölz, S., Hopper, J.R., Ion, G., León, R., Magalhaes, V., Makovsky, Y., Mata, M.-P., Max, M.D., Nielsen, T., Okay, S., Ostrovsky, I., O'Neill, N., Pinheiro, L.M., Plaza Faverola, A.A., Rey, D., Roy, S., Schwalenberg, K., Senger, K., Vadakkepuliyambatta, S., Vasilev, A., Vázquez, J.T., 2020. Hydrate occurrence in Europe: A review of available evidence, Marine and Petroleum Geology, 111, 735-764, doi:10.1016/j.marpetgeo.2019.08.014

Naudts, L., Greinert, J., Artemov, Y., Staelens, P., Poort, J., Van Rensbergen, P., De Batist, M., 2006. Geological and morphological setting of 2778 methane seeps in the Dnepr paleo-delta, northwestern Black Sea, Marine Geology, 227, 177-199, https://doi.org/10.1016/j.margeo.2005.10.005

Öszoy, E., Ünlüata, Ü., 1997. Oceanography of the Black Sea: a review of some recent results, Earth-Science Reviews 42, 231-272, doi:10.1016/S0012-8252(**97**)81859-4.

Pape T., Bahr A., Rethemeyer J., Kessler J.D., Sahling H., Hinrichs K.-U., Klapp S.A., Reeburgh W.S., Bohrmann G., 2010. Molecular and isotopic partitioning of low-molecular weight hydrocarbons during migration and gas hydrate precipitation in deposits of a high-flux seepage site, Chemical Geology, 269, 350-363, doi: 10.1016/j.chemgeo.2009.10.009

Pape, T., Bahr, A., Klapp, S.A., Abegg, F., & Bohrmann, G., 2011. High-intensity gas seepage causes rafting of shallow gas hydrates in the southeastern Black Sea, Earth and Planetary Science Letters, 307, 35–46, https://doi.org/10.1016/j.epsl.2011.04.030.

Pape, T., Haeckel, M., Riedel, M., Kölling, M., Schmidt, M., Wallmann, K., Bohrmann, G., 2020. Formation pathways of light hydrocarbons in deep sediments of the Danube Deep-sea fan, Western Black Sea, Marine and Petroleumn Geology, 122, 104627, Special Issue Black Sea Gas Hydrates, https://doi.org/10.1016/j.marpetgeo.2020.104627

Pfender, M., & Villinger, H., 2002. Miniaturized data loggers for deep sea sediment temperatur gradient measurements, Marine Geology, 186, 557-570, doi:10.1016/S0025-3227(02)00213-X

Plaza-Faverola, A., Vadakkepuliyambatta, S., Hong, W.-L., Mienert, J., Bünz, S., Chand, S., Greinert, J., 2017. Bottom simulating reflector dynamics at Arctic thermogenic gas provinces: An example from Vestnesa ridge, offshore west Svalbard, Journal of Geophysical Research Solid Earth, 122, 4089–4105 https://doi.org/10.1002/2016JB013761

Popescu, I., De Batist, M., Lericolais, G., Nouzé, H., Poort, J., Panin, N., Versteeg, W., & Gillet, H., 2006. Multiple bottom-simulating reflections in the Black Sea: Potential proxies of past climate conditions, Marine Geology, 227, 163-176, https://doi.org/10.1016/j.margeo.2005.12.006

Popescu, I., Lericolais, G., Panin, N., De Batist, M., Gillet, H., 2007. Seismic expression of gas and gas hydrates across the western Black Sea, Geo-Marine Letters 27, 173-183, https://doi.org/10.1007/s00367-007-0068-0

Riboulot, V., Cattaneo, A., Scalabrin, C., Gaillot, A., Jouet, G., Ballas, G., Marsset, T., Garziglia, S., Ker, S., 2017. Control of the geomorphology and gas hydrate extent on widespread gas emissions offshore Romania, Bull. Soc. géol. Fr., 188(4), 26p., https://doi.org/10.1051/bsgf/2017182.

Riboulot, V., Ker, S., Sultan, N., Thomas, Y., Marsset, B., Scalabrin, C., Ruffine, L., Boulart, C., Ion, G., 2018. Freshwater lake to salt-water sea causing widespread hydrate dissociation in the Black Sea, Nature Communications, 9(1). https://doi.org/10.1038/s41467-017-02271-z

Riedel, M., Wallmann, K., Berndt, C., Pape, T., Freudenthal, T., Bergenthal, M., Bünz, S., Bohrmann, G., 2018. In-situ temperature measurements at the Svalbard continental margin: implications for gas hydrate dynamics, Geochemistry, Geophysics, Geosystems, 19(4), 1165-1177, https://doi.org/10.1002/2017GC007288

Riedel, M., Freudenthal, T., Bergenthal, M., Haeckel, M., Wallmann, K., Spangenberg, E., Bialas, J., Bohrmann, G., 2020. Physical Properties and core-log seismic integration from drilling at the Danube Deep sea fan, Black Sea, Marine Petroleum Geology, 114, 104192, Special Issue Black Sea Gas Hydrates, https://doi.org/10.1016/j.marpetgeo.2019.104192

Römer, M., Sahling, H., dos Santos Ferreira, C., Bohrmann, G., 2020. Methane gas emissions of the Black Sea—mapping from the Crimean continental margin to the Kerch Peninsula slope. Geo-Marine Letters 40, 467-480. doi:10.1007/s00367-019-00611-0.

Ross, D. A., Neprochnov, Y. P., et al., 1978. Initial Reports of the Deep Sea Drilling Project, Volume 42, Part 2: Washington (U.S. Government Printing Office).

Ruppel, C., 1997. Anomalously cold temperatures observed at the base of the gas hydrate stability zone, U.S. Atlantic passive margin, Geology, 25, 699–702, doi:10.1130/0091-7613(1997)025<0699:ACTOAT>2.3.CO;2.

Schowalter, T.T., 1979. Mechanics of secondary hydrocarbon migration and entrapment. AAPG Bull., 63(5):723–760

Shipley, T.H., Houston, M.H., Buffler, R.T., Shaub, F.J., McMillen, K.J., Ladd, J.W., Worzel, J.L., 1979. Seismic evidence for widespread possible gas hydrate horizons on continental slopes and rises. AAPG Bulletin 63, 2204-2213, https://doi.org/10.1306/2F91890A-16CE-11D7-8645000102C1865D

Soulet, G., Delaygue, G., Vallet-Coulomb, C., Böttcher, M.E., Sonzogni, C., Lericolais, G., Bard, E., 2010. Glacial hydrologic conditions in the Black Sea reconstructed using geochemical pore water profiles, Earth and Planetary Science Letters, 296(1-2), 57-66, https://doi.org/10.1016/j.epsl.2010.04.045

Soulet, G., Ménot, G., Lericolais, G., Bard, E., 2011. A revised calendar age for the last reconnection of the Black Sea to the global ocean. Quaternary Science Reviews, 30(9-10), 1019–1026. https://doi.org/10.1016/j.quascirev.2011.03.001

Spence, G.D., Haacke, R., Hyndman, R.D., 2010. Seismic indicators of natural gas hydrates and underlying free gas, in: Riedel, Willoughby, Chopra (eds): Geophysical Development Series No. 14, Geophysical Characterization of Gas Hydrates, Society of Exploration Geophysicists, 39-71, https://doi.org/10.1190/1.9781560802197.ch4.

Tishchenko, P., Hensen, C., Wallmann, K., Wong, C.S., 2005. Calculation of the stability and solubility of methane hydrate in seawater, Chemical Geology, 219(1-4), 35-52, https://doi.org/10.1016/j.chemgeo.2005.02.008

Torres, M.E., Teichert, B.M.A., Tréhu, A.M., Borowski, W., Tomaru, H., 2004. Relationship of pore water freshening to accretionary processes in the Cascadia margin: fluid sources and gas hydrate abundance. Geophys. Res. Lett., 31:L22305. doi:10.1029/2004GL021219 .

Vassilev, A., Dimitrov, L.I., 2002. Spatial and quantity evaluation of the Black Sea gas hydrates, Russian Geology and Geophysics, 43, 672-684.

Vasilev, A., 2015. Geothermal evolution of gas hydrate deposits: Bulgarian exclusive economic zone in the Black Sea. Comptes rendus de l'Académie bulgare des sciences: sciences mathématiques et naturelles, 68(9), 1135-1144.

Yefremova, A.G., Zhizchenko, B.P., 1974. Occurrence of crystal hydrates of gases in the sediments of modern marine basins. Akademii Nauk SSSR 214, 1179-1181

Zander, T., Haeckel, M., Berndt, C., Chi, W.-C., Klaucke, I., Bialas, J., Klaeschen, D., Koch S., Atgin, O., 2017. On the origin of multiple BSRs in the Danube deep-sea fan, Black Sea, Earth and Planetary Science Letters, 462, 15 – 25, doi: 10.1016/j.epsl.2017.01.006

Supporting Information

In this supplement, we show the raw temperature records of each measurement-process made with the MTL-tool in situ (Figure S1). The temperature record of the MTL during the entire drilling process is shown in Figure S2, illustrating temperature variations throughout the complete coring and drilling process.

Figure S3 provides a collage of seismic data across the S2 channel providing a tie between the two main drill-holes MeBo-17 (west) and MeBo-16 (east).

Figures S4 and S5 are additional seismic images of the newly developed bottom-simulating reflection (here referred to as BSR-0).

Figure S6 is a snapshot of rising gas bubbles from the borehole at MeBo-17 when the drill bit was at the depth of the seismically imaged BSR-1 at around 144 mbsf.

Table S1 provides detailed data of in situ temperatures measured at MeBo-17.

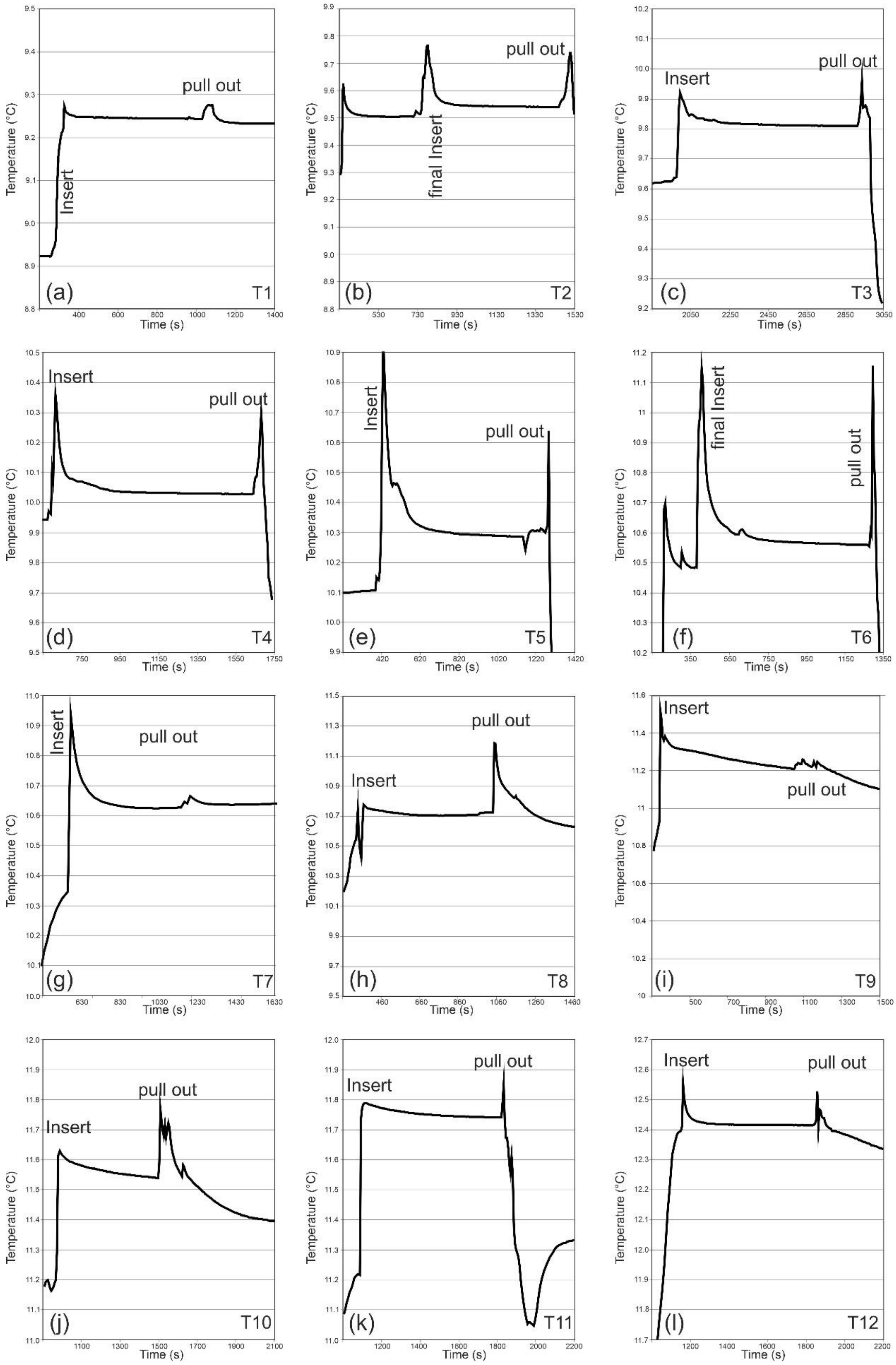

Figure S1 (a) – (l): Temperature records of deployments of the MTL at Site MeBo-17. Times of insertion into sediment and pull-out are indicated.

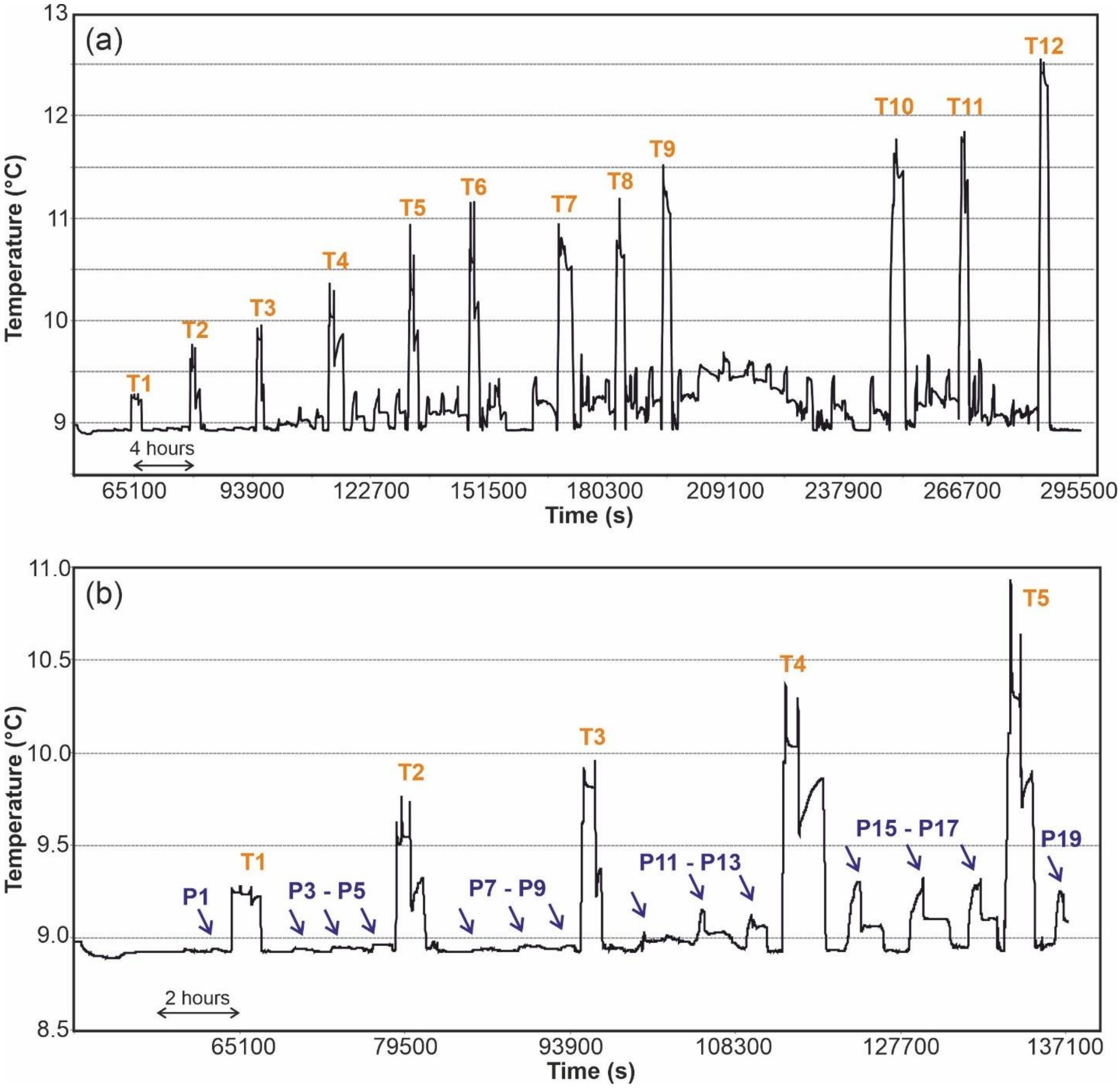

Figure S2 (a) Image showing the temperature measured with the MTL during the entire drilling process at Site MeBo-17. Twelve insertions of the tool were made (T1 – T12). The tool was stored in the MeBo200 rig while coring operations were conducted. The movement of core barrels also affects the temperature at the MTL, but temperature does cool down to bottom-water levels regularly. (b) Detailed view for the period of the first five temperature measurements (T1 – T5) and core-barrel runs (P1 – P19).

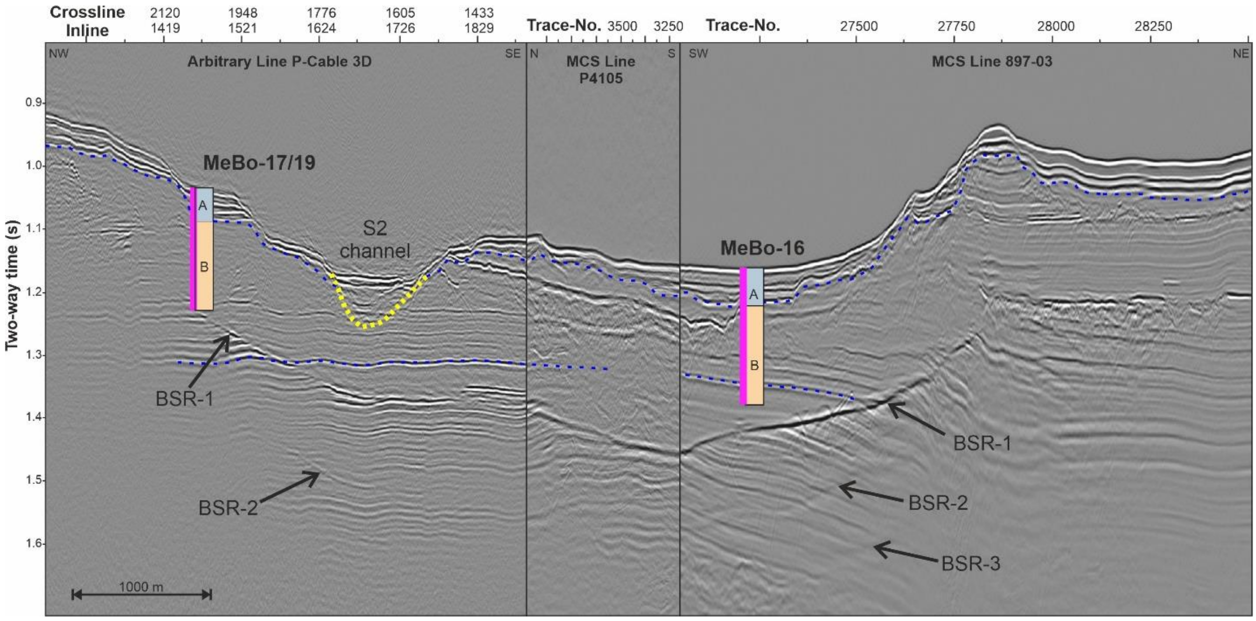

Figure S3 Splice of seismic sections through the MeBo-16 and MeBo-17 drill sites. Simplified stratigraphy of Unit A and Unit B are included with key stratigraphic horizons marked as blue dashed lines (modified from Riedel et al., 2020). The main BSR-1 is regionally imaged. Deeper paleo-BSRs (BSR-2, BSR-3) can be seen only locally. Note, the frequency difference in the P-cable and MCS data from using different seismic sources results in different imaging character of the subsurface along the section.

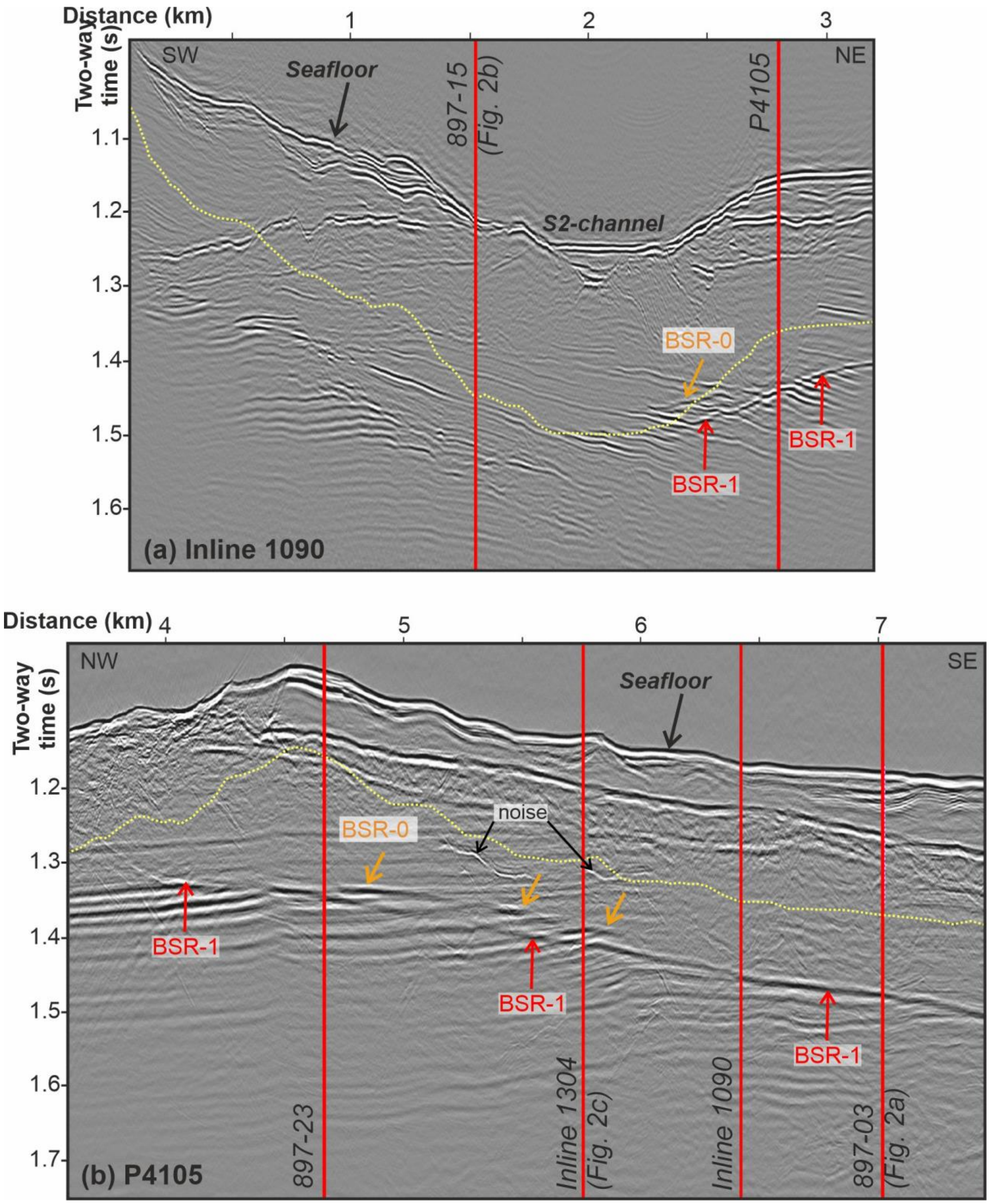

Figure S4 Examples of high-frequency seismic data from expedition MSM34 at the S2-Channel region. (a) Inline 1090 from P-Cable 3D data, and (b) MCS line P4105 along the western shoulder of the levee of the S2-channel. Here, only BSR-1 (red) and the shallower BSR-0 (orange) are seen. Yellow dotted line is base of gas hydrate stability (1D model) given today's conditions based on MeBo drilling. Location of lines see Figure 1.

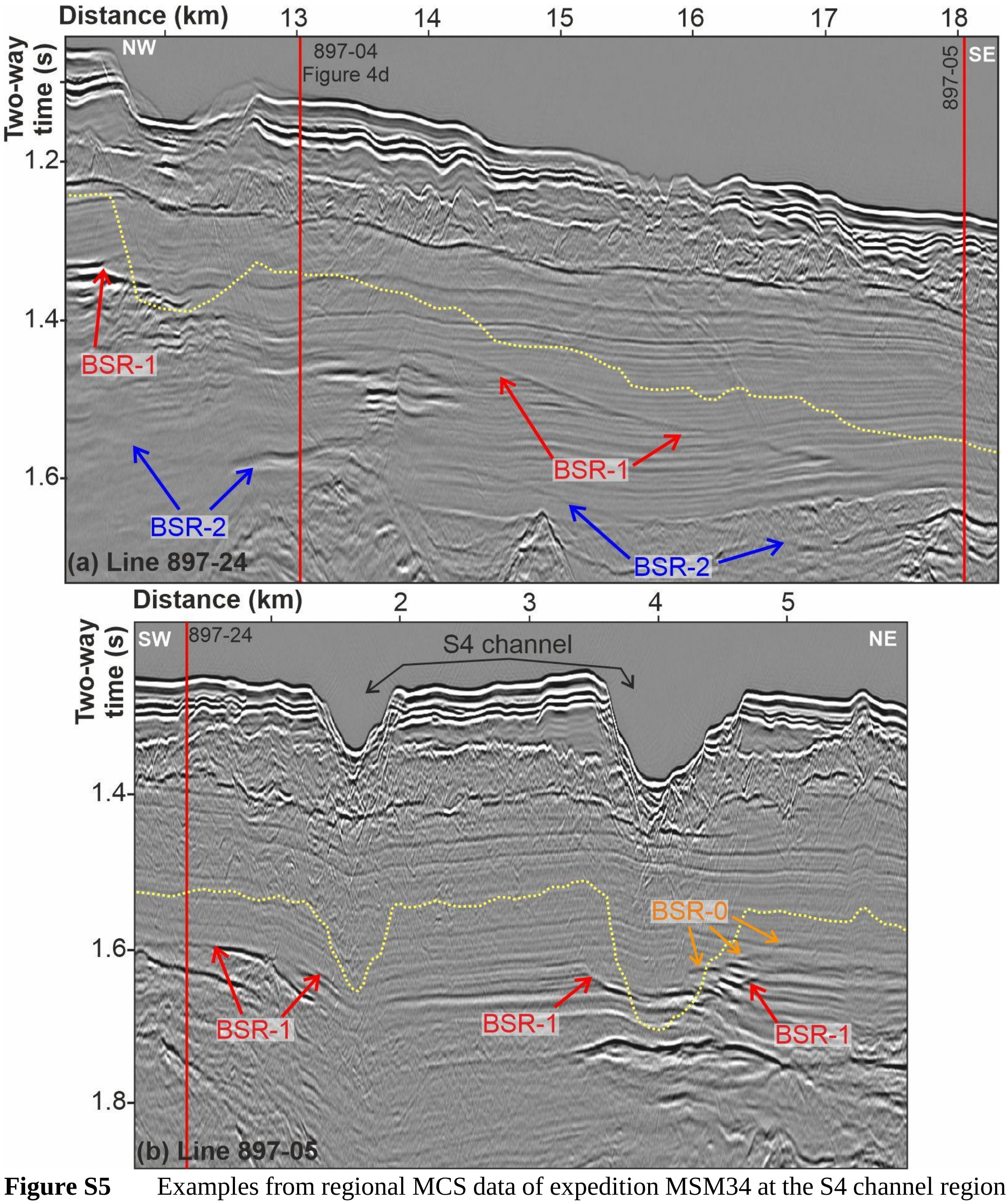

Figure S5 Examples from regional MCS data of expedition MSM34 at the S4 channel region: (a) line 897-24 showing a wide-spread BSR-1 and BSR-2, (b) line 897-05, crossing the meandering talweg of the S4-channel twice. Here, only BSR-1 is seen, together with a shallower BSR-0 (orange arrows). Yellow dotted line is base of gas hydrate stability (1D model) given today's conditions based on MeBo drilling. Location of lines see Figure 1.

Figure S6 Image taken from the inside of the MARUM MeBo200 drill rig frame when performing operations at Site GeoB22605-1 (MeBo17). The photo was taken on November 19, 2017 when drilling reached a depth of 143.85 mbsf, close to the expected depth of the BSR-1. Free gas bubbles escaped from the borehole (examples indicated by red arrows) and deeper drilling was stopped.

Table S1. In situ temperature data from Site MeBo-17 (GeoB22605-1) and MeBo-18 (GeoB22609-1). The maximum possible penetration (and thus maximum distance to top of exposed sediment and minimum effect of the cooling) for the MTL is 15.5 cm.

Site	Depth below seafloor (m)	Time of exposure (min)	Insertion depth of sensor (mm)	Correction applied (°C)	Initial estimated temperature (°C)	Adjusted in situ temperature (°C)
MeBo-17 GeoB22605-1	7.35	39	155	0.018	9.243	9.261
	17.85	30	138	0.018	9.541	9.559
	28.35	30	130	0.020	9.811	9.831
	38.85	46	131	0.026	10.030	10.056
	49.35	41	119	0.027	10.287	10.314
	59.85	48	98	0.029	10.559	10.588
	70.35	97	132	0.042	10.626	10.668
	80.85	28	140	0.034	10.727	10.761
	91.35	40	133	0.038	11.211	11.249
	115.85	75	121	0.049	11.54	11.589
	126.35	44	135	0.048	11.742	11.790
	143.85	41	134	0.051	12.416	12.467
MeBo-18 GeoB22609-1	14.35	53	143	0.022	9.498	9.520